

# This is a JAM - Just Accepted Manuscript

## Journal of Porphyrins and Phthalocyanines

**Article Title:** Construction of Secondary Coordination Sphere Boosts Electrochemical CO<sub>2</sub> Reduction of Iron Porphyrins

**Author(s):** Guiyu Liu, Ying-Jie Fan, Jun-Long Zhang

**DOI:** 10.1142/S1088424619501608

### To be cited as:

Guiyu Liu, Ying-Jie Fan, Jun-Long Zhang, Construction of Secondary Coordination Sphere Boosts Electrochemical CO<sub>2</sub> Reduction of Iron Porphyrins, *Journal of Porphyrins and Phthalocyanines*, doi: 10.1142/S1088424619501608

**Received:** 3 September, 2019

**Accepted:** 8 October, 2019

This is the accepted and unedited version of a newly accepted manuscript after peer-review evaluation. No copyediting, typesetting or proof correction has been performed, so it is by no means the definitive final version of the manuscript. This format allows a rapid display online with a DOI, which means that the manuscript is already citable in a sustainable manner.

It has been uploaded in advance for the benefit of our customers. The manuscript will be copyedited, typeset and proofread before it is released in the final form. As a result, the published copy may differ from the unedited version. Readers should obtain the final version from the above link when it is published. The authors are responsible for the content of this Accepted Article.

When the corrected proof will be available, the manuscript will move to the Online Ready page of the website. The definitive version with page numbers will be available after publication of the issue in which it takes place.

Thanks to this free and optional opportunity, the newly accepted manuscript can be quickly shared with the scientific community.

In no case, WorldScientific can be held responsible of mistakes in the content of use of this Just Accepted Manuscript.

# Construction of Secondary Coordination Sphere Boosts Electrochemical CO<sub>2</sub> Reduction of Iron Porphyrins

Guiyu Liu<sup>a</sup>, Ying-Jie Fan<sup>a</sup>, and Jun-Long Zhang<sup>a\*</sup>

<sup>a</sup>Beijing National Laboratory for Molecular Sciences, State Key Laboratory of Rare Earth Materials Chemistry and Applications, College of Chemistry and Molecular Engineering, Peking University, Beijing 100871, P. R. China.

**ABSTRACT:** Inspired by the biological NiFe CO dehydrogenase that hydrogen bond donors exist in the secondary sphere to enhance the CO<sub>2</sub> reduction activity, iron porphyrins with simple aminophenyl substitution are synthesized and their electrochemical CO<sub>2</sub> reduction properties are studied. **Fe-1**, bearing amino group in the *ortho* position of the phenyl ring exhibits the improved catalytic turn over frequency (TOF), lower overpotential, and higher selectivity, compared with *para*-amino-substituted iron porphyrin (**Fe-2**) and the control Fe-TPP (**Fe-3**). DFT calculation also supports that importance of hydrogen bond on the reactivity of **Fe-1** facilitates the formation [Fe-CO<sub>2</sub>]<sup>2-</sup> adduct by lowering 1.45 kcal/mol.

**KEYWORDS:** Secondary coordination sphere, CO<sub>2</sub> reduction, hydrogen bond, porphyrin

\*Correspondence to: Jun-Long Zhang, email: zhangjunlong@pku.edu.cn, fax: +86 10-62767034

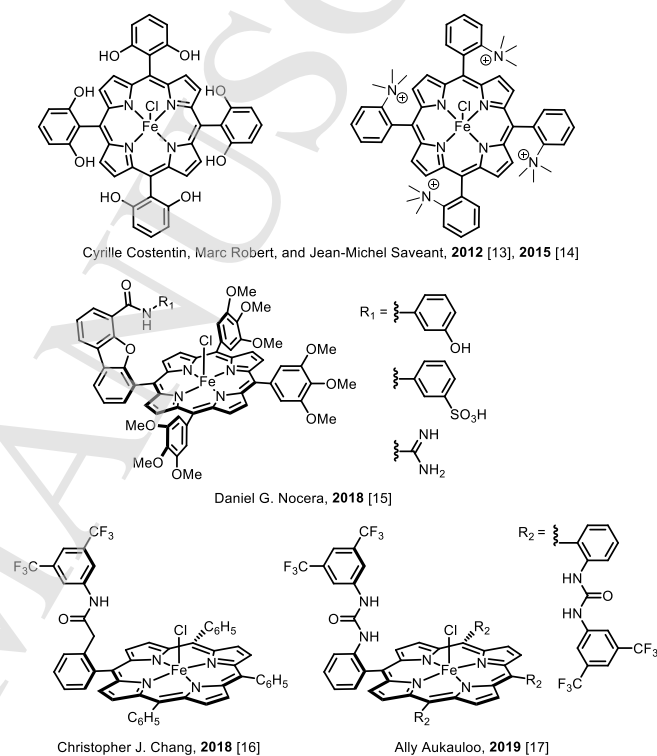
## INTRODUCTION

The rising atmospheric CO<sub>2</sub> concentration causes climate change and ocean acidification, along with many other environmental changes. Many approaches have been developed to convert CO<sub>2</sub> into high value-added chemical products.[1-3] Among them, electrochemical reduction of CO<sub>2</sub> can be a candidate to meet the challenge, but direct CO<sub>2</sub> reduction is both kinetic and thermodynamic unfavourable. Rational design of catalysts is highly required to promote the efficiency and selectivity in CO<sub>2</sub> fixation and reduction.

In biological system, carbon monoxide dehydrogenase (CODH) enzymes can reversibly catalyze the reduction of CO<sub>2</sub> to CO. In the typical Ni-Fe CODH example, the precise position of histidine and lysine residues is critical to construct the secondary sphere providing hydrogen-bond and proton-relay groups to stabilize the CO<sub>2</sub>-metal intermediate.[1,4] Recent advances have been reported in metal catalyzing CO<sub>2</sub> activation with the assistance of secondary intramolecular hydrogen bond.[5-7] For examples, amines[8,9], carboxylic acids[10], imidazolium moieties[11] and thiourea tethers[12] have been used as hydrogen-bond donors or acceptors to construct the secondary coordination sphere, which have been found to improve the electrocatalytic activity and decreased significantly the overpotential of the metal catalysts. Among them, metal porphyrins have been broadly reported for CO<sub>2</sub> electrochemical reduction as molecular catalysts, and some of examples are shown in **Scheme 1**. Savéant, Costentin, and Robert reported phenol[13] and ammonium cations[14] pendant enhance CO<sub>2</sub> reduction efficiencies in the Fe porphyrins. Iron haptophan porphyrins with phenol and guanidinium groups reported by Nocera et al. also showed catalytic enhancement.[15] Chang and Nichols have investigated the positional dependence of secondary coordination sphere on the reactivity of electrochemical CO<sub>2</sub> reduction by proximal and distal amide groups.[16] Most recently, Aukauloo and Halime reported four urea functions that provide a multipoint hydrogen bond donors at a Fe porphyrin, which demonstrates a remarkable drop of the

overpotential and a high turnover frequency.[17] These pioneering studies revealed the importance of positioning secondary coordination sphere in CO<sub>2</sub> reduction and further exploring a simple approach to construct such secondary sphere would be of importance for CO<sub>2</sub> reduction.

**Scheme 1.** Reported CO<sub>2</sub> reduction catalysts by iron porphyrins with the assistance of secondary coordination sphere.



Herein, we introduce a molecular model bearing amino groups at *meso*-phenyl group. Compared their electrochemical CO<sub>2</sub> reduction properties with iron tetraphenylporphyrin catalyst (FeTPP), the *ortho* amino substituted iron porphyrin exhibits enhanced catalytic activity (TOF = 10<sup>4</sup> s<sup>-1</sup>). DFT calculations show hydrogen bond between the amino donor and the [Fe-CO<sub>2</sub>]<sup>2-</sup> adduct stabilizes the intermediate.

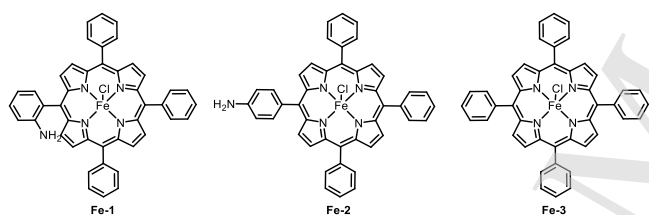
## RESULTS AND DISCUSSION

### Synthesis and characterization

5-(*o*-Aminophenyl)-10,15,20-triphenylporphyrin (*o*-NH<sub>2</sub>TPP),  
 5-(*p*-Aminophenyl)-10,15,20-triphenylporphyrin (*p*-NH<sub>2</sub>TPP) tetra(*meso*-phenyl)porphyrin (TPP) were synthesized according to

literature procedure.[18,19] The corresponding iron complexes, **Fe-1**, **Fe-2**, **Fe-3**, as shown in **Scheme 2**, were prepared by refluxing excess anhydrous iron(II) chloride in dry DMF under  $N_2$  atmosphere, and treated with LiCl. The identity of each free-base porphyrin was confirmed by  $^1H$  NMR spectroscopy and high-resolution mass spectrometry. The UV-vis absorption spectra and cyclic voltammetry (CV) were used to probe the optical and electrochemical properties of these iron complexes. Regarding the UV-vis spectra of **Fe-1** and **Fe-3**, the Soret bands wavelength were observed at 414 nm in dichloromethane. Relative to **Fe-1** and **Fe-3**, the absorption of **Fe-2** was slightly red-shift to 417 nm. The same optical changes were observed with Q-bands absorption. The origin of the red-shift may attributed to the electron-donating *para*-amino group in the porphyrin backbone.

**Scheme 2.** Structure of **Fe-1**, **Fe-2** and **Fe-3**.



### Cyclic voltammetry studies

CVs of Fe complexes in argon degassed DMF containing 0.1 M of tetra-*N*-butylammonium hexafluorophosphate ( $nBu_4NPF_6$ ) are shown in **Fig. 1**. **Fe-3** shows three redox waves at  $E_{1/2} = -0.667$ ,  $-1.494$ , and  $-2.119$  V versus  $Fc^{+/0}$ , corresponding to formal  $Fe^{III/II}$ ,  $Fe^{II/I}$ , and  $Fe^{I/0}$  couples.[20] Comparable redox events are observed for **Fe-1** ( $E_{1/2} = -0.682$ ,  $-1.508$ , and  $-2.147$  V) and **Fe-2** ( $E_{1/2} = -0.710$ ,  $-1.556$ , and  $-2.201$  V); and each reduction is cathodically shifted relative to **Fe-3**. The third redox wave of **Fe-2** (characteristic of  $CO_2$  reduction onset potential,  $E_{cat}^0$ ) shifts almost 80 mV to more negative potential compared with those of **Fe-1** and **Fe-3**, indicating that higher overpotential can be observed in  $CO_2$  reduction. This shift can attribute to the donating effect of the  $-NH_2$  groups on the aryl ring. The *ortho* substituted **Fe-1** shows anodic shifts compared to the *para* substituted **Fe-2**, which indicates that the proximal amino

group in **Fe-1** facilitates metal reduction through hydrogen bond compared with distal amino group for **Fe-2**. Scan rate-dependence studies show a linear correlation between peak current and  $(\text{scan rate})^{1/2}$ , indicating that all the redox events occurred are diffusion controlled under non-catalytic conditions (**Fig. S1-2**).

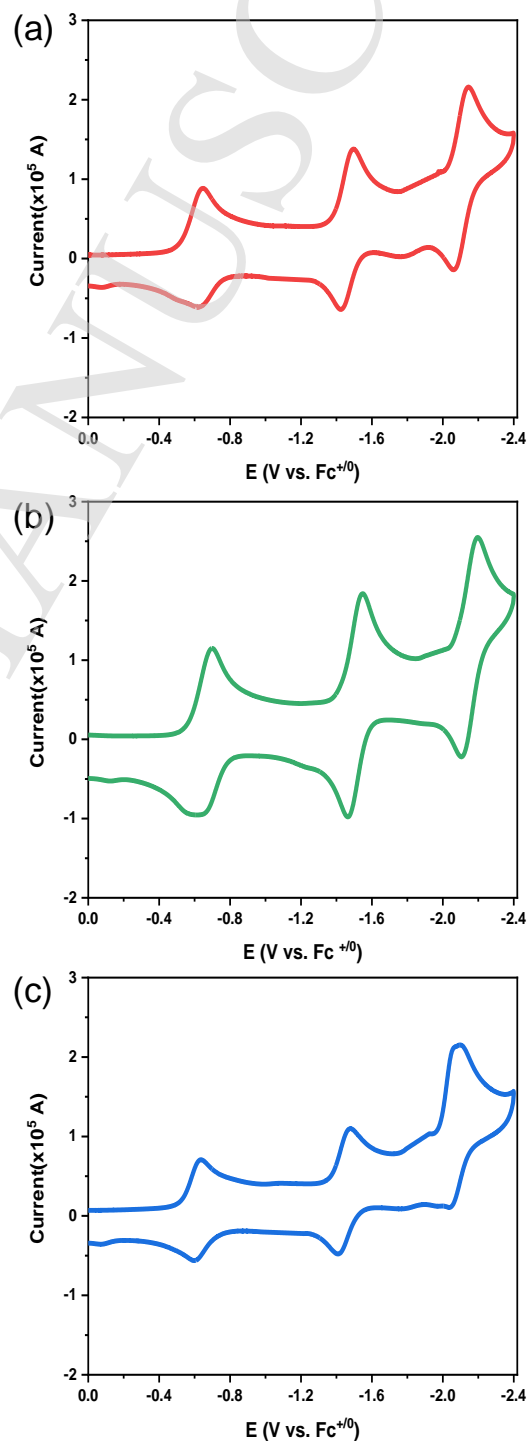


**Fig. 1.** CVs of 1 mM **Fe-1**, **Fe-2** and **Fe-3** in DMF containing 0.1 M  $nBu_4NPF_6$  under Ar. Conditions: 1 mM catalyst, 0.1 M  $nBu_4NPF_6$  in DMF under Ar; scan rate is 100 mV/s.

## Electrochemical CO<sub>2</sub> reduction

The CO<sub>2</sub> reduction capability of the three Fe complexes is evaluated by successive cyclic voltammograms in CO<sub>2</sub>-saturated DMF. The CVs of **Fe-1**, **Fe-2**, and **Fe-3** show only moderate current enhancement near the third reduction wave at  $E_{cat/2} = -2.110$ ,  $-2.123$ ,  $-2.175$  V respectively (**Fig. 2**). To increase the catalytic activity, weak Brønsted acids such as phenol which was served as the proton source was added to the solution. In the presence of phenol, an S-shaped irreversible catalytic response is observed for the three iron complexes, as shown in **Fig. 2**.

The catalytic rates for **Fe-1**, **Fe-2**, and **Fe-3** are extracted using the plateau peak current under CO<sub>2</sub> with

phenol ( $i_{cat}$ ), relative to the peak current of the noncatalytic redox process under argon ( $i_p$ ) using eqn (1): [21]

$$TOF = \frac{Fvn_p^3}{RT} \left( \frac{0.4463}{n_{cat}} \right)^2 \left( \frac{i_{cat}}{i_p} \right)^2 \quad (1)$$

where  $F$  is the Faraday constant,  $n_p$  is the number of electrons transferred in the redox event,  $F$  the Faraday constant,  $R$  is the universal gas constant,  $T$  is the temperature,  $n_{cat}$  is the number of electrons required for the catalytic reaction ( $n_{cat} = 2$ ). We note that the use of eqn (1) is restricted to ideal S-shaped voltammograms. The calculated TOFs for the three Fe complexes in different concentration of phenol are shown in **Fig. 2** (d).

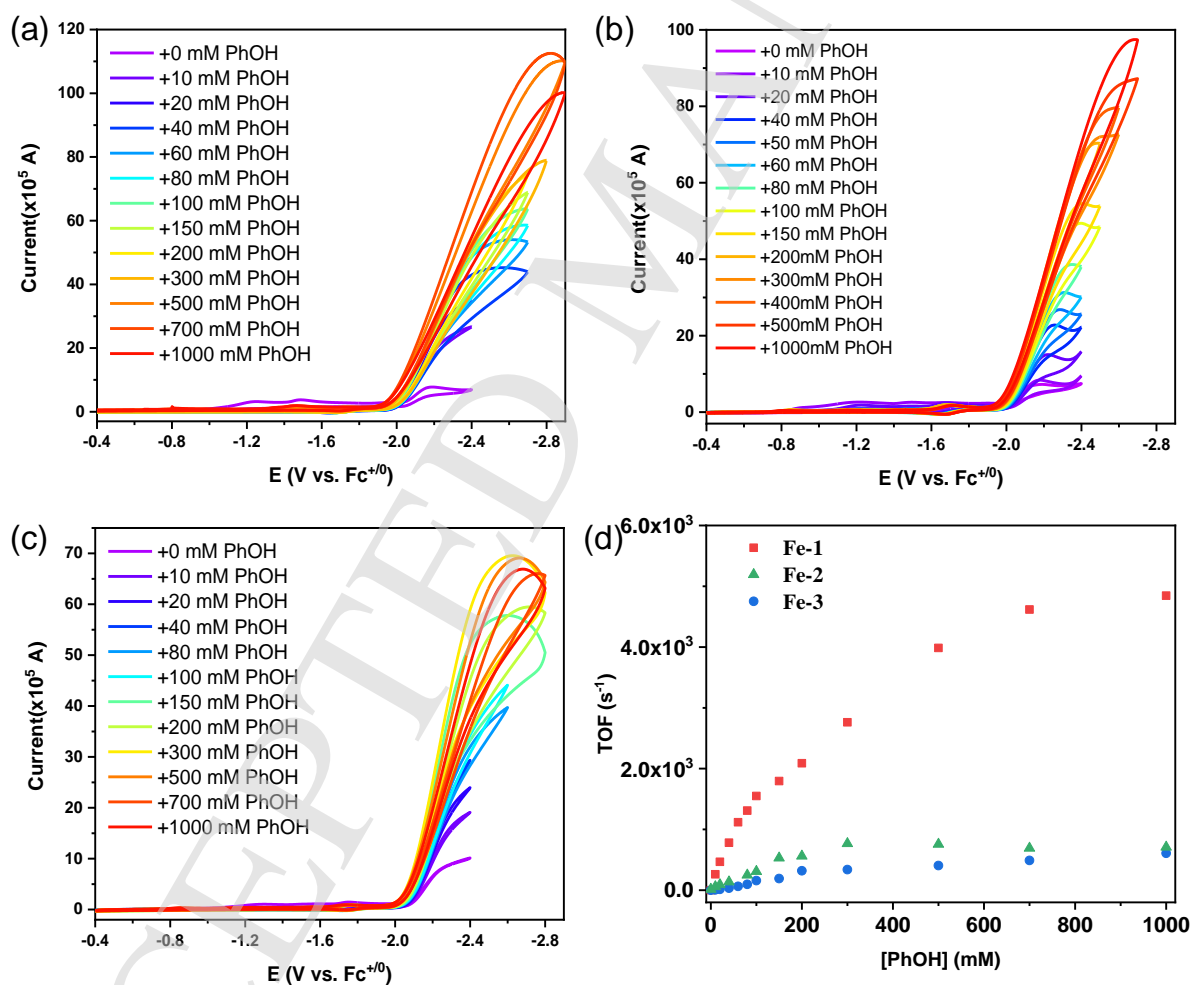


**Fig.2.** CVs of 1 mM **Fe-1** (a), **Fe-2** (b) and **Fe-3** (c) in DMF containing 0.1 M nBu<sub>4</sub>NPF<sub>6</sub> under CO<sub>2</sub> with different phenol concentration. (d) TOF for catalytic CO<sub>2</sub> reduction under different concentration of phenol. Conditions: 1 mM catalyst, 0.1 M nBu<sub>4</sub>NPF<sub>6</sub> in DMF; 0.23 M CO<sub>2</sub>; scan rate is 100 mV/s.

Under the pseudo-first order conditions, the catalytic rates of all the three catalysts display first-order dependence on phenol concentration at low acid concentrations, but exhibit non-linear relationship under higher phenol concentrations. **Fe-1** displays significantly enhanced catalytic reactivity up to a maximum turnover frequency (TOF) of 4846 s<sup>-1</sup>, which is ca. 7 times greater than that of **Fe-2** (710 s<sup>-1</sup>) and **Fe-3** (608 s<sup>-1</sup>) under 1 M phenol. Thus, these results demonstrate that hydrogen-bond interaction with amino groups in the secondary sphere of iron porphyrin can remarkably enhance catalytic CO<sub>2</sub> reduction reactivity.

Given the nonideal behavior, Costentin and Savéant's [22] foot-of-the-wave analysis (FOWA) is also adopted via eqn (2) to determine intrinsic catalytic rates:

$$\frac{i_{cat}}{i_p} = \frac{2.24 \sqrt{\frac{RT}{Fv}} k_{obs}}{1 + \exp\left[\frac{F}{RT}(E - E_{cat}^0)\right]} \quad (2)$$

**Table 1.** Summary of the electrochemical properties of Fe complexes.

catalyst	$E_{1,1/2}^a/V$	$E_{2,1/2}^a/V$	$E_{3,1/2}^a/V$	TOF <sup>b</sup> /s <sup>-1</sup>	TOF <sub>FOWA</sub> <sup>c</sup> /s <sup>-1</sup>	TON <sup>d</sup>
<b>Fe-1</b>	-0.682	-1.508	-2.147	4846	10443	21
<b>Fe-2</b>	-0.710	-1.556	-2.201	710	2535	11
<b>Fe-3</b>	-0.667	-1.494	-2.119	608	1035	13

<sup>a</sup> vs. Fc<sup>+/0</sup>. <sup>b</sup> TOF values are reported in presence of 1 mM catalyst, 1 M PhOH and 0.23 M CO<sub>2</sub> in DMF based on the  $i_{cat}/i_p$  methods. <sup>c</sup> TOF<sub>FOWA</sub> values are reported in presence of 0.5 M PhOH and 0.23 M CO<sub>2</sub> in DMF based on FOW analysis. <sup>d</sup> in 3 h based on the actual amount of CO.

For the purposes of catalyst benchmarking, it is illustrative to examine the relationship between log(TOF) and overpotential ( $\eta = E_{cat}^0 - E_{CO_2/CO}^0$ ) as indicated by a catalytic Tafel plot.[23] As is shown in **Fig. 3**, **Fe-1** exhibits higher TOF compared to **Fe-2** and **Fe-3**. The overpotential of **Fe-1** is lower than that of **Fe-2** (ca. 80 mV), owing to the secondary sphere amino of *ortho*-substituted porphyrin.

In this electroanalytical method, the competing factors such as substrate depletion and catalyst inhibition were minimized by analyzing the foot of the catalytic wave to determine the observed catalytic rate constant ( $k_{obs}$ ). From plots of  $i_{cat}/i_p$  versus  $1/\{1 + \exp[(F/RT)(E - E_{cat}^0)]\}$ ,  $k_{obs}$  could be calculated from the slope of the linear portion of the curve and provides an access to the maximum TOF ( $k_{obs} = TOF_{max}, s^{-1}$ ) (**Fig. S3**). The TOF<sub>FOWA</sub> for **Fe-1**, **Fe-2** and **Fe-3** are 10443, 2535 and 1035 s<sup>-1</sup> respectively in 0.5 M phenol (**Table 1**). Despite of different results obtained from two methods, the similar trend that amino groups in the secondary sphere of iron enhance the catalytic activity was observed. Thus, hydrogen bond formed between the amino group and the [Fe-CO<sub>2</sub>]<sup>2-</sup> is supposed to stabilize the intermediate in the CO<sub>2</sub> reduction process.

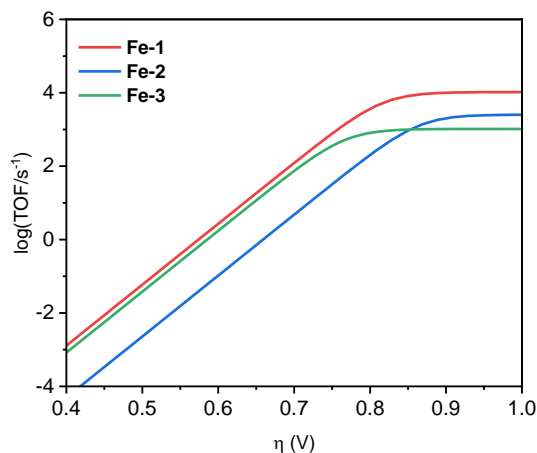


**Fig. 3.** Catalytic Tafel plots of the Fe porphyrins (1 mM) in 0.5 M phenol.

To estimate the selectivity and stability of the aforementioned catalysts, the controlled potential electrolysis (CPE) was performed at  $-2.3$  V vs.  $\text{Fc}^{+/0}$  in  $\text{CO}_2$  saturated DMF electrolyte with  $0.4$  M phenol as proton source for the three complexes (**Fig. 4**). In the two-compartment cell using a standard three-electrode setup, **Fe-1** achieved a maximum Faradaic efficiency (FE) of 88% for CO. CO was the major product observed by GC over the 3 h test period. The total turnover number of CO ( $\text{TON}_{\text{CO}}$ ) for **Fe-1** was 21 based on the actual amount of catalyst. As for **Fe-2** and **Fe-3**, the maximum FE of CO was similar as **Fe-1** *ca.* 87%, and the hydrogen was the minor gas product for the two complexes with FE of *ca.* 2%. The TON of CO of **Fe-2** and **Fe-3** was only 11 and 13 respectively. The TONs here are based on the actual amount of CO during the bulky electrolysis, and the TOF mentioned before extracted from cyclic voltammetry curves is based on the catalyst in the diffusion layer. Therefore there remains large gap between the TON and TOF.

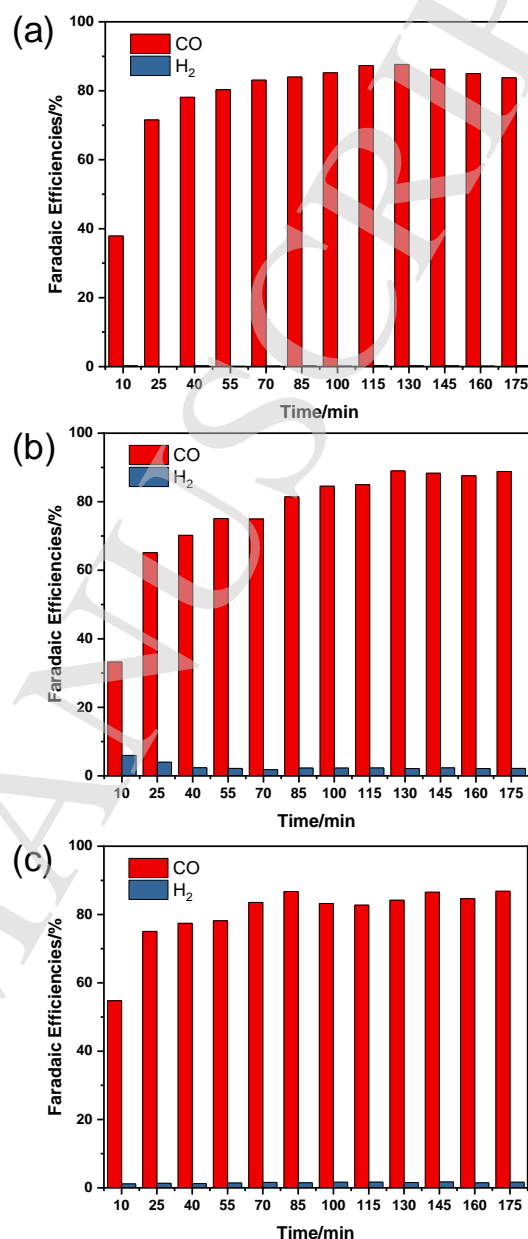
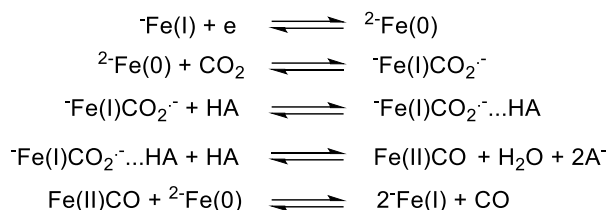


**Fig.4.** Faradaic efficiencies for  $\text{H}_2$  and CO for **Fe-1** (a), **Fe-2** (b) and **Fe-3** (c). Conditions: 1 mM catalyst, 0.1 M  $n\text{Bu}_4\text{NPF}_6$  in DMF with 0.23 M  $\text{CO}_2$  0.4 M phenol at  $-2.3$  V vs.  $\text{Fc}^{+/0}$ .

#### DFT calculated $\text{CO}_2$ binding process

The catalytic reduction of  $\text{CO}_2$  to CO is a two-electron coupling two-proton process, and the mechanism is shown as **Scheme 3**.<sup>[24]</sup> The catalytic cycle is initiated by reduction of Fe(I) to Fe(0) species, followed by the binding of  $\text{CO}_2$  and formed the  $[\text{Fe-CO}_2]^{2-}$  adduct as the key intermediate. For **Fe-1**, we hypothesized that this adduct is strongly stabilized by intramolecular hydrogen bonding with the pendant  $\text{NH}_2$  groups and carried out DFT calculations to verify.

**Scheme 3.** Proposed mechanism for electrochemical reduction of CO<sub>2</sub> by Fe porphyrins with Brønsted acids (HA).



The binding event is calculated for the three Fe porphyrins. The triply reduced Fe(0)-CO<sub>2</sub> species possess a -2 charge and triplet state is the most stable among the three spin states ( $S = 0$ , singlet;  $S = 1$ , triplet and  $S = 2$ , quintuplet). In contrast with CO<sub>2</sub> ( $d(\text{CO}) = 1.117 \text{ \AA}$  and  $\text{OCO} = 180.0^\circ$ ) and radical anion CO<sub>2</sub><sup>-</sup> ( $d(\text{CO}) = 1.235 \text{ \AA}$  and  $\text{OCO} = 127.0^\circ$ ), upon bind to Fe(0), the bond length of CO is  $1.242 \text{ \AA}$  and O-C-O is bent to  $135.6^\circ$ . These results indicate CO<sub>2</sub> is reduced to CO<sub>2</sub><sup>-</sup> by the iron catalyst. For **Fe-1**, the Mulliken charge of iron atom is +0.33, revealing that the iron atom possesses a slightly positive charge. In the case of **Fe-1**, a hydrogen-bond interaction between the amino group in the *ortho*-aryl ring and the coordinated CO<sub>2</sub> substrate is found with N(H)⋯O donor-acceptor distances of  $1.972 \text{ \AA}$  (**Fig. 5**). In contrast, **Fe-2** and **Fe-3** cannot form similar hydrogen bond. The distance of Fe and C atom of the CO<sub>2</sub> for **Fe-1** is  $2.024 \text{ \AA}$  while the distance for **Fe-3** is  $2.078 \text{ \AA}$ . In contrast, **Fe-2** and **Fe-3** cannot form similar hydrogen bond. The free energy of stabilization the [Fe-CO<sub>2</sub>]<sup>2-</sup> adduct for **Fe-2** is  $1.45 \text{ kcal mol}^{-1}$  compared with **Fe-3**, thus illustrating the large stabilizing effect of the -NH<sub>2</sub> groups upon binding the carbon dioxide to Fe(0).

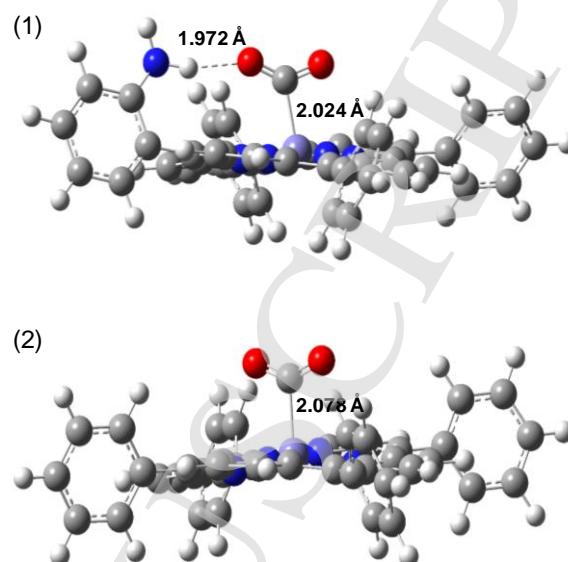


**Fig.5.** Structure models of [CO<sub>2</sub>-Fe]<sup>2-</sup> adducts for **Fe-1** (a) and **Fe-3** (b).

## CONCLUSION

Taken together, inspired by the natural carbon monoxide dehydrogenase that hydrogen bond donors in the secondary coordination sphere, we designed and synthesized simple *ortho* and *para* substituted amino iron porphyrins model, **Fe-1** and **Fe-2** respectively. As shown by the electrochemical measurements, **Fe-1** exhibits a significant rate acceleration ( $\text{TOF} = 10^4 \text{ s}^{-1}$ ), 4 times to **Fe-2**, and 10 times to **Fe-3**. **Fe-1** also shows high CO selectivity. Faradaic efficiencies of CO for **Fe-1** reach to 88% with little hydrogen ( $\text{FE} < 0.5\%$ ) evolution. Computational results demonstrate N-H adjacent to the bent CO<sub>2</sub> stabilize the intermediate by forming hydrogen bond. These studies highlight the importance of the secondary coordination sphere and the position of hydrogen bond donors in the catalytic reduction of CO<sub>2</sub>.

## EXPERIMENTAL

### General procedures

Commercially available solvents were being purified by the MBraun SPS-800 Solvent Purification System. Tetrabutylammonium hexafluorophosphate (*n*Bu<sub>4</sub>NPF<sub>6</sub>) was recrystallized from absolute ethanol. Other reagents were purchased from commercial suppliers and used

without purification. UV-vis spectra were recorded on an Agilent 8453 UV-vis spectrometer. ESI-MS were recorded on a Bruker APEX IV Fourier Transform Ion Cyclotron Resonance Mass Spectrometer using electrospray ionization.  $^1\text{H}$  and  $^{13}\text{C}$  NMR spectra were recorded on a Bruker-400 MHz NMR. All  $^1\text{H}$  NMR experiments were reported in  $\delta$  units, parts per million (ppm), and all coupling constants were in Hz and measured relative to the signal for residual chloroform (7.26 ppm) in the deuterated solvent  $\text{CDCl}_3$ . Cyclic voltammetry experiments were recorded on Shanghai Chenhua CHI660C electrochemical workstation. A glassy carbon electrode was selected as the working electrode, the auxiliary electrode was a platinum wire electrode and  $\text{Ag}/\text{AgCl}$  was the reference electrode. All samples were recorded in  $N,N$ -dimethylformamide (DMF) with 0.1 M  $n\text{Bu}_4\text{NPF}_6$  as the electrolyte. Unless otherwise noted, the scan rate was  $0.1 \text{ V s}^{-1}$ , and all potentials in this study were adjusted to the ferrocenium/ferrocene ( $\text{Fc}^{+/0}$ ) couple as an internal standard. The potential for  $\text{Fc}^{+/0}$  couple vs  $\text{Ag}/\text{AgCl}$  (3 M KCl) is 0.50 V in DMF. All GC spectrometry experiments were measured and recorded using GC-2014 (Shimadzu, Japan).

### Controlled Potential Electrolysis (CPE)

All CPE experiments were performed with a gas-tight two-compartment H-shaped cell, and a glassy carbon plate (1 cm x 1 cm) was used as the working electrode, along with a Pt-wire counter electrode and a nonaqueous  $\text{Ag}/\text{AgCl}$  reference electrode. Two solutions were prepared: a work solution (0.5 mM catalyst + 0.1 M  $n\text{Bu}_4\text{NPF}_6$  + 0.5 M phenol), and a blank solution (0.1 M  $n\text{Bu}_4\text{NPF}_6$  + 0.5 M phenol). The glassy carbon plate working electrode and reference electrode were immersed in the work solution in the cathodic compartment, while the counter electrode was immersed in the blank solution in the anodic compartment.

$\text{CO}_2$  was first allowed to flow through the working compartment at a rate of  $40 \text{ mL min}^{-1}$  for 30 min and then the flow rate of  $\text{CO}_2$  was changed to  $5 \text{ mL min}^{-1}$ . Cyclic voltammetry (CV) was carried out at a scan rate of  $0.1 \text{ V s}^{-1}$ . During chronoamperometry, the effluent gas from the

cell was introduced directly into the gas sample loop of gas chromatograph (GC) for gas analysis. The gas chromatograph equipped with two of Porapak-N, MS-13X and HP-AL/S columns was used for quantifications. The gas-phase product was analyzed by GC every 15 min. CO in the gas products was analyzed using a thermal conductivity detector (TCD) with  $\text{H}_2$  as a carrier gas, whereas  $\text{H}_2$  in the gas products was analyzed using another TCD with  $\text{N}_2$  as a carrier gas, and the alkanes in the gas products were analyzed using a flame ionization detector (FID) with  $\text{N}_2$  as a carrier gas. The liquid products were characterized by  $^1\text{H}$  NMR spectra, in which 0.1 mL electrolyte was mixed with 0.4 mL DMF, and 0.1  $\mu\text{L}$  benzene was added as an internal standard. The amount of charge passed to produce each product was divided by the total charge passed at a specific time or during the overall run to evaluate each FE, seeing supporting information in detail.

### Computational details

All geometry optimization calculations were performed using the density functional theory (DFT) at the BP86/6-311G(d,p) [25-27] level in the Gaussian 09 software.[28] The solvent effect was considered in all geometry optimizations using the conductor-like polarizable continuum model (CPCM). Thermodynamic quantities were calculated for  $T = 298 \text{ K}$ .

### Acknowledgements

We thank the National Scientific Foundation of China (NSFC) (21571007, 21621061, 21778002, 21861162008) and the National Key Basic Research Support Foundation of China (NKBRFC) (2015CB856301) for financial support. And this work was supported by High-performance Computing Platform of Peking University.

### REFERENCES

1. Appel AM, Bercaw JE, Bocarsly AB, Dobbek H, DuBois DL, Dupuis M, Ferry JG, Fujita E, Hille R, Kenis PJ, Kerfeld CA, Morris RH, Peden CH, Portis AR, Ragsdale SW, Rauchfuss TB, Reek JN, Seefeldt LC, Thauer RK and Waldrop GL. *Chem. Rev.* 2013; **113**: 6621-6658.

2. Benson EE, Kubiak CP, Sathrum AJ and Smieja JM. *Chem. Soc. Rev.* 2009; **38**: 89-99.
3. Morris AJ, Meyer GJ and Fujita E. *Acc. Chem. Res.* 2009; **42**: 1983-1994.
4. Can M, Armstrong FA and Ragsdale SW. *Chem. Rev.* 2014; **114**: 4149-4174.
5. Dutta A, Appel AM and Shaw WJ. *Nat. Rev. Chem.* 2018; **2**: 244-252.
6. Cook SA and Borovik AS. *Acc. Chem. Res.* 2015; **48**: 2407-2414.
7. Rakowski Dubois M and Dubois DL. *Acc. Chem. Res.* 2009; **42**: 1974-1982.
8. Chapovetsky A, Welborn M, Luna JM, Haiges R, Miller TF and Marinescu SC. *ACS Cent. Sci.* 2018; **4**: 397-404.
9. Roy S, Sharma B, Pecaut J, Simon P, Fontecave M, Tran PD, Derat E and Artero V. *J. Am. Chem. Soc.* 2017; **139**: 3685-3696.
10. Neri G, Aldous IM, Walsh JJ, Hardwick LJ and Cowan AJ. *Chem. Sci.* 2016; **7**: 1521-1526.
11. Sung S, Kumar D, Gil-Sepulcre M and Nippe M. *J. Am. Chem. Soc.* 2017; **139**: 13993-13996.
12. Haviv E, Azaiza-Dabbah D, Carmieli R, Avram L, Martin JML and Neumann R. *J. Am. Chem. Soc.* 2018; **140**: 12451-12456.
13. Costentin C, Drouet S, Robert M and Savéant JM. *Science* 2012; **338**: 90-94.
14. Costentin C, Robert M, Savéant JM and Tatin A. *Proc. Natl. Acad. Sci. USA* 2015; **112**: 6882-6886.
15. Margarit CG, Schnedermann C, Asimow NG and Nocera DG. *Organometallics* 2018; **38**: 1219-1223.
16. Nichols EM, Derrick JS, Nistanaki SK, Smith PT and Chang CJ. *Chem. Sci.* 2018; **9**: 2952-2960.
17. Gotico P, Boitrel B, Guillot R, Sircoglou M, Quaranta A, Halime Z, Leibl W and Aukauloo A. *Angew. Chem. Int. Ed.* 2019; **58**: 4504-4509.
18. Luguya R, Jaquinod L, Fronczek FR, Vicente MGH and Smith KM. *Tetrahedron* 2004; **60**: 2757-2763.
19. Filhoa CS, Ferreirab AG, Gotardoa AF and Marilda DA. *J. Porphyrins Phthalocyanines* 2005; **9**: 637-645.
20. Hammouche M, Lexa D, Momenteau M and Savéant JM. *J. Am. Chem. Soc.* 1991; **113**: 8455-8466.
21. Francke R, Schille B and Roemelt M. *Chem. Rev.* 2018; **118**: 4631-4701.
22. Costentin C, Drouet S, Robert M and Savéant JM. *J. Am. Chem. Soc.* 2012; **134**: 11235-11242.
23. Costentin C and Savéant JM. *Nat. Rev. Chem.* 2017; **1**: 0087.
24. Costentin C, Passard G, Robert M and Savéant JM. *J. Am. Chem. Soc.* 2014; **136**: 11821-11829.
25. Wu YY, Rodriguez-Lopez N and Villagran D. *Chem. Sci.* 2018; **9**: 4689-4695.
26. Hariharan PC and Pople JA. *Theor. Chim. Acta* 1973; **28**: 213-222.
27. Francl MM, Petro WJ, Hehre WJ, Binkley JS, Gordon MS, DeFree DJ and Pople JA. *J. Chem. Phys.* 1982; **77**: 3654-3665.
28. Frisch MJ, Trucks GW, Schlegel HB, Scuseria GE, Robb MA, Cheeseman JR, Scalmani G, Barone V, Mennucci B, Petersson GA, Nakatsuji H, Caricato M, Li X, Hratchian HP, Izmaylov AF, Bloino J, Zheng G, Sonnenberg JL, Hada M, Ehara M, Toyota K, Fukuda R, Hasegawa J, Ishida M, Nakajima T, Honda Y, Kitao O, Nakai H, Vreven T, Montgomery JA, Peralta J, J. E., Ogliaro F, Bearpark M, Heyd JJ, Brothers E, Kudin KN, Staroverov VN, Kobayashi R, Normand J, Raghavachari K, Rendell A, Burant JC, Iyengar SS, Tomasi J, Cossi M, Rega N, Millam JM, Klene M, Knox JE, Cross JB, Bakken V, Adamo C, Jaramillo J, Gomperts R, Stratmann RE, Yazyev O, Austin AJ, Cammi R, Pomelli C, Ochterski JW, Martin RL, Morokuma K, Zakrzewski VG, Voth GA, Salvador P, Dannenberg JJ, Dapprich S, Daniels AD, Farkas Ö, Foresman JB, Ortiz JV, Cioslowski J and Fox DJ. *Gaussian 09 (Revision E.01)*; Gaussian Inc.: Wallingford CT, 2009